INSTITUTE OF PHYSICS PUBLISHING JOURNAL OF PHYSICS B: ATOMIC, MOLECULAR AND OPTICAL PHYSICS

J. Phys. B: At. Mol. Opt. Phys. **36** (2003) 4289–4299 PII: S0953-4075(03)65286-7

Low energy differential and integral electron-impact cross sections for the $2s^2 2p^4\ ^3P \rightarrow 2p^3 3s\ ^3S^o$ excitation in atomic oxygen

P V Johnson[1], I Kanik[1], M A Khakoo[2], J W McConkey[3] and S S Tayal[4]

[1] Jet Propulsion Laboratory, California Institute of Technology, 4800 Oak Grove Drive, Pasadena, CA 91109, USA
[2] Department of Physics, California State University, Fullerton, CA 92634, USA
[3] Department of Physics, University of Windsor, Windsor, ON, N9B 3P4, Canada
[4] Department of Physics, Clark Atlanta University, Atlanta, GA 30314, USA

Received 24 June 2003
Published 14 October 2003
Online at stacks.iop.org/JPhysB/36/4289

Abstract

Differential and integral cross sections (ICSs) for $2s^2 2p^4\ ^3P \rightarrow 2p^3 3s\ ^3S^o$ excitation in atomic oxygen have been measured at electron-impact energies of 15, 17.5, 20, 22.5 and 27.5 eV. Differential measurements were conducted with a conventional electron energy-loss spectrometer and a microwave discharge source of atomic oxygen. Relative differential cross sections (DCSs) were determined between 15 and 30 eV impact energy. With the help of theoretical predictions of the shape of the DCS at large angles, measured results were extrapolated to 180° scattering angle and relative ICSs were deduced. The relative excitation function was normalized to the 30 eV impact energy ICS given by Kanik *et al* (2001 *J. Phys. B: At. Mol. Opt. Phys.* **34** 2647). Normalization of the ICS values allowed the measured DCSs to be put on the absolute scale. Theoretical calculations of the DCSs were carried out using the R-matrix with the pseudostates approach. A total of 22 spectroscopic bound and autoionizing states, together with 19 pseudostates, were included in the close-coupling expansion. The pseudostates were chosen to simulate continuum target states. Theoretical results, along with other available experimental data, have been compared with the current experimental results.

1. Introduction

Atomic oxygen is one of the most abundant elements in the universe and its various emission lines are prominent in Earth's airglow and aurora as well as the atmospheres of Mars, Venus and elsewhere. These emissions may be produced by collisions with electrons either deposited from the solar wind or released via photo-ionization processes. Clearly, there is much need for accurate cross sections in order to model and interpret these observations. To this end, a number

of works have been published that present measurements of both excitation and emission cross sections. A detailed summary of past atomic oxygen work is presented in Kanik *et al* (2001). More recently, Johnson *et al* (2003) have measured emission cross sections from threshold to 1 keV for the 130.4, 102.7, 98.9 and 87.8 nm emission lines while Tayal (2002) has calculated integral cross sections (ICSs) for the direct excitation of the $2p^3 3s\ ^3S^o$ and $2p^3 3d\ ^3D^o$ states.

Despite the volume of work that has been done, there remains a conspicuous lack of experimental data for the direct excitation of atomic oxygen in the important low, near threshold region. This lack of experimental data is particularly acute in the case of the $2s^2 2p^4\ 3P \rightarrow 2p^3 3s\ ^3S^o$ transition, which is arguably the most important resonant transition in the O I system, yielding the 130.4 nm emission triplet. To date, the only near threshold measurements of direct $2p^3 3s\ ^3S^o$ excitation are given by Vaughan and Doering (1987), Gulcicek and Doering (1988) and Doering and Yang (2001). At 30, 50 and 100 eV, the cross sections of Vaughan and Doering (1987) and Kanik *et al* (2001) agree remarkably well. However, the lower energy cross sections of Gulcicek and Doering (1988) and Doering and Yang (2001) are considerably larger than the other measurements from this group where overlap occurs in the data sets. This has led Doering and Yang (2001) to suggest a 'best guess' excitation function. In the light of this situation, it is clear that further work is needed in order to confirm our understanding of $2s^2 2p^4\ ^3P \rightarrow 2p^3 3s\ ^3S^o$ excitation in the low energy regime.

2. Experimental procedures and analysis

Kanik *et al* (2001) have previously described the apparatus and many of the experimental procedures used in the current measurements. Therefore, only a brief summary will be given here with some elaboration on the details specific to this work. The reader is referred to Kanik *et al* (2001) for further details of the current procedures and to Trajmar and Register (1984) and Trajmar and Kanik (1995) for general information on determining differential cross sections (DCSs) and ICSs via electron energy-loss spectroscopy.

The electron energy-loss spectrometer consists of an electron gun, a scattered electron detector and a target beam of atomic oxygen in a crossed-beam arrangement. During the current experiments, the spectrometer was tuned to achieve an overall system energy resolution of about 90 meV full width at half-maximum (FWHM). The only change in the apparatus since the earlier work of Kanik *et al* (2001), apart from the addition of some differential pumping to the electron gun to extend the filament lifetime, was in regards to the oxygen source. In the present work, atomic oxygen was produced in an extended microwave discharge cavity fed with a mixture of 90% O_2 and 10% He. This differed from the work in Kanik *et al* (2001) where a 95% O_2 and 5% N_2 feed was used. This was to avoid any complications of the spectra due to the presence of N_2, N, N^+ etc in the beam. After leaving the discharge tube, the O, O_2 and He mixture was transported through a Teflon tube to a quartz needle, from which the target beam effused into the interaction region. The needle itself was coated in a conductive 'silver paint' and was grounded to prevent any charge accumulation and subsequent introduction of electric fields into the collision region.

Initial attempts at low energy oxygen cross section measurements were made using the beam-chopping scheme for background signal determination described by Kanik *et al* (2001). Unfortunately, this technique was unable to properly account for the background signals at the current energies due to scattering of electrons from the beam chopper. Therefore, the oxygen source was modified to facilitate the measurement of background signals as follows. The gas needle was held in a Teflon cylinder, fixed within a pivoting aluminium sleeve. The sleeve was mounted in such a fashion that, when aligned with the scattering centre, the sleeve was in firm contact with a 'stop' located above the pivot point. A stepper-motor-controlled

rocker arm, attached to the aluminium sleeve below the pivot point by means of a 'spring', was used to change the direction of the gas beam. Limit switches, connected to the stepper motor controller, were used to set the two extremes of the rocker arm's motion. At one extreme, the spring would torque the aluminium sleeve against the stop and the needle would be aligned with the scattering centre (i.e. the '*beam*' position). On moving the rocker arm to its opposite extreme, the spring would torque the needle, about the pivot, away from the previously aligned position so that the gas beam was directed away from the scattering centre (i.e. the '*background*' position). In this way, background measurements could be taken without changing the flow rate of gas into the experimental chamber. Hughes *et al* (2003) detail the operational principles of such movable target sources for accurate background determination in electron scattering experiments.

Given the fact that the cross sections vary sharply with impact energy at the low energies involved in the current investigation, it was particularly important to accurately calibrate the absolute impact energy. This was done using the He $2\,^2S$ elastic scattering resonance at 19.37 eV. This calibration was repeated periodically throughout the data acquisition phase of the work. The reported impact energies are accurate to within ± 0.02 eV.

The Kanik *et al* (2001) analysis relied on the dissociation fraction of the source, derived from O_2 feature intensities measured with the discharge on and off, for normalization of the measured cross sections. In the present work, a simpler approach was taken. Experience with microwave discharge atomic oxygen production (Kanik *et al* 2001, Noren *et al* 2001, Johnson *et al* 2003) has led to the conclusion that the dissociation fraction is both stable and reproducible given consistent operating conditions of the discharge source (discharge pressure, microwave power etc). During the current experiments, great care was taken to ensure such consistent operating conditions and, for that reason, a constant dissociation fraction has been assumed throughout. The ICS for the $2s^2 2p^4\ ^3P \rightarrow 2p^3 3s\ ^3S^o$ transition at 30 eV impact energy can be considered well established based on the results of Kanik *et al* (2001) and Vaughan and Doering (1987) who reported ICSs that agreed to within 5%. Therefore, the assumption of constant dissociation fraction and the existence of an atomic oxygen normalization standard made the determination of relative and subsequently absolute DCSs and ICSs possible without explicit determination of the dissociation fraction. This eliminated the complication of taking spectra with the discharge off as was required in Kanik *et al* (2001). A detailed description of the normalization procedure employed is given in section 3.

At each incident energy, energy-loss data were taken at 5° intervals from 0° to 25°. At the larger scattering angles, it was considered best to use the calculated shape of the DCS to estimate the contribution to the ICS. This was due to the rapid fall-off of the DCS with scattering angle and an increasing level of contamination by molecular background features close to 9.5 eV energy loss at angles $>25°$. Background signals were measured concurrently with the data in an automated fashion by alternating the gas needle between the '*beam*' and '*background*' positions as discussed previously. As we were particularly interested in $2p^3 3s\ ^3S^o$ excitation (9.51 eV energy loss), spectra were restricted to the 9–10.5 eV energy-loss range. This greatly expedited the acquisition process and enabled the required statistical accuracy ($<2\%$) to be obtained in time periods that were not prohibitively long.

3. Data analysis

In order to obtain relative DCSs, one needs to measure scattering intensities as a function of energy and angle under identical conditions such as target gas pressure, gun and detector tuning, and electron beam current. In practice, however, this is more difficult than the above statement implies. Therefore, it is desirable to derive the relative DCSs from a ratio of feature intensities

taken from the same spectrum. In such a situation, all multiplicative factors mentioned above cancel and thereby make an experiment impervious to drifting of such parameters during data acquisition. Kanik *et al* (2001) gave the absolute DCS of an atomic oxygen feature, a, as

$$\mathrm{DCS_a} = \frac{(1-D)}{\sqrt{2}D}\frac{I_{\mathrm{a}}^{\mathrm{on}}}{I_{\mathrm{LB}}^{\mathrm{on}}}\mathrm{DCS_{LB}} \tag{1}$$

where D is the dissociation fraction of the source, $I_{\mathrm{a}}^{\mathrm{on}}$ is the intensity of the atomic oxygen feature, $I_{\mathrm{LB}}^{\mathrm{on}}$ is the intensity of a molecular oxygen feature (here the so-called 'longest band' is indicated by LB) and $\mathrm{DCS_{LB}}$ is the DCS of the molecular feature (the superscript 'on' indicates the state of the discharge source). As mentioned previously, the dissociation fraction has been assumed to be constant throughout the current measurements. Furthermore, Shyn *et al* (1994) and Johnson and Kanik (2001) have determined DCSs of the LB in O_2 over the range of energies and angles covered in the present study. Therefore, relative DCSs could be determined as follows:

$$\mathrm{DCS_a^{rel}} = \frac{I_{\mathrm{a}}^{\mathrm{on}}}{I_{\mathrm{LB}}^{\mathrm{on}}}\mathrm{DCS_{LB}}. \tag{2}$$

This determination exploits the advantages associated with analysing intensity ratios, as discussed above.

At each energy and angle, spectra were taken with the gas needle in the *beam* and *background* positions over an energy-loss range that included both the $2p^3 3s\ ^3S^o$ atomic and LB molecular excitations. By subtracting the *background* spectra from the appropriate *beam* spectra, the $2p^3 3s\ ^3S^o$ atomic and LB molecular excitations were isolated from any background signal as discussed in Kanik *et al* (2001). Integrated intensities of the energy-loss features were then determined and relative $2p^3 3s\ ^3S^o$ DCSs were derived according to equation (2). As mentioned previously, Shyn *et al* (1994) and Johnson and Kanik (2001) have measured $\mathrm{DCS_{LB}}$ over the energy range (15–30 eV) appropriate to the present work. Very good agreement between the two data sets was obtained over all overlapping angles and energies. However, DCSs were not available at all required combinations of impact energy and scattering angle. Therefore, it was necessary to interpolate between actual quoted values to obtain values at some of the required combinations of impact energy and scattering angle.

The validity of the analysis outlined above is contingent on the O_2 rovibrational distribution in the collision region being equivalent to that in the experiments of Shyn *et al* (1994) and Johnson and Kanik (2001) where conventional room temperature gas jets were employed. In the current experiments, all species leaving the discharge region travelled a distance of approximately 30 cm through a Teflon tube ($\sim$0.5 Torr) before effusing from a room temperature quartz needle into the collision region. As such, oxygen molecules experienced a large number of collisions as they travelled between the discharge and collision regions. These collisions ensured the relaxation of any rovibrational populations that may have been excited in the discharge. This assertion is supported by comparisons of energy-loss spectra taken with the discharge on and off which show O_2 feature intensities occurring in identical proportions under either discharge condition. We therefore conclude that the O_2 rovibrational population distributions were the same/similar in both the current experiments and those of Shyn *et al* (1994) and Johnson and Kanik (2001) and that the outlined analysis was legitimate. Further discussion regarding the composition of target beams produced by atomic oxygen microwave discharge sources is given by Kanik *et al* (2001) and Johnson *et al* (2003).

Relative ICSs were obtained by extrapolating the relative DCSs to 180° and then integrating over all angles. Having established the relative DCS at angles below 25° where the majority of the contributions to the integrated cross section lie, we chose to estimate the cross sections at larger angles using our theoretical DCSs to guide the procedure. Thus, we applied a scaling

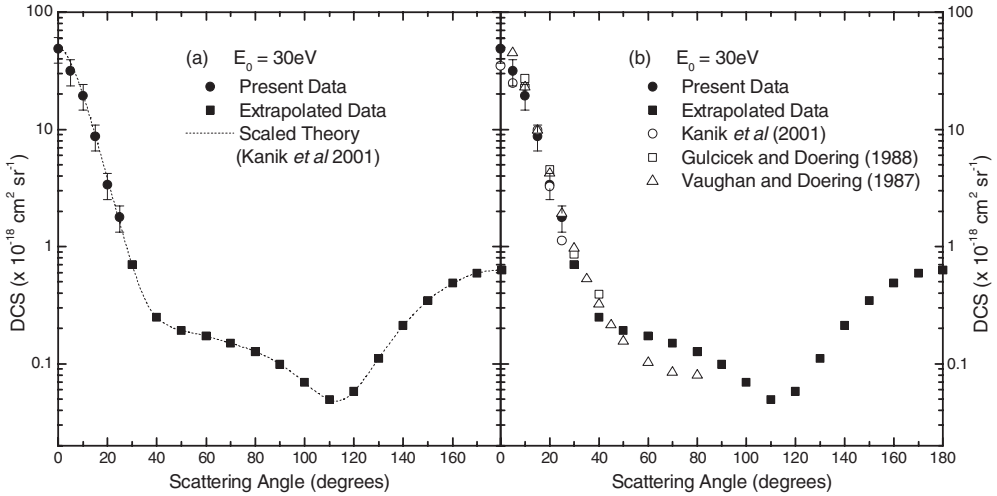

Figure 1. Normalized experimental DCSs for $2s^2 2p^4\ ^3P \rightarrow 2p^3 3s\ ^3S^o$ excitation at 30 eV impact energy. The measured and extrapolated DCSs are shown in panel (a) along with the relative *R*-matrix DCSs of Kanik *et al* (2001) (scaled to the present experimental results as discussed in the text). The experimental results of Vaughan and Doering (1987), Gulcicek and Doering (1988) and Kanik *et al* (2001) are shown alongside the present data in panel (b).

factor to the theoretical data to bring them into agreement with the experimental data in the 0°–25° scattering region and then used the modified theoretical data at the larger angles to guide the extrapolation. This is well justified, given the very good agreement between the shapes of the experimental and theoretical data in the low angle region (0°–25°). Numerical integration of the data was then performed to produce a relative $2p^3 3s\ ^3S^o$ excitation function. The excitation function was normalized at 30 eV to the ICS given by Kanik *et al* (2001). Therefore, absolute ICSs for the $2p^3 3s\ ^3S^o$ excitation were determined. We note that the *R*-matrix DCS results of Kanik *et al* (2001) were employed in the extrapolation of the 30 eV experimental DCSs as no new theoretical DCSs were calculated at this energy. Figure 1 shows the experimentally determined absolute 30 eV DCSs along with the extrapolated large angle DCSs. The relative *R*-matrix DCSs of Kanik *et al* (2001) (scaled to the present experimental results as discussed above) are also shown to demonstrate how theory was used to guide the high angle extrapolation of the DCSs. The experimentally determined DCSs of Vaughan and Doering (1987), Gulcicek and Doering (1988) and Kanik *et al* (2001) are presented in the figure for comparison.

The scaling factor used to normalize the ICSs was then applied to the relative DCSs putting them on the absolute scale as well. It is of note, since relative DCSs were determined according to equation (2), that the normalization factor applied to the data was equal to the $(1 - D)2^{-1/2}D^{-1}$ factor found in equation (1). Therefore the dissociation fraction of the oxygen source could be calculated and was found to be 0.32. This result is consistent with our previous experience (Kanik *et al* 2001, Noren *et al* 2001, Johnson *et al* 2003).

In the current analysis, only the relative shapes of the LB DCSs played a role and not the absolute values. Therefore, the uncertainty in these DCSs associated with normalization can be neglected in the current work (14%—Shyn *et al* (1994); 12–14%—Johnson and Kanik (2001)). Removing these uncertainties from the quoted errors leaves relative uncertainties of 11% and 9–12% in the Shyn *et al* (1994) and Johnson and Kanik (2001) data sets, respectively. Given the relative uncertainties in these data and the excellent level of agreement between the two

data sets, an uncertainty of 10% has been attributed to the relative LB DCSs. An uncertainty of 10% is attributed to the extrapolation of the relative DCSs as discussed in Kanik *et al* (2001) while statistical uncertainties were <2%. Normalization to the 30 eV ICS value of Kanik *et al* (2001) provided the largest contribution to the overall uncertainty. Kanik *et al* (2001) quoted an uncertainty of 29%. However, the excellent agreement between Kanik *et al* (2001) and Vaughan and Doering (1987) for the 30 eV ICS suggests that the 30 eV ICS is established to an absolute accuracy of no worse than 20%. Adding these uncertainties in quadrature yields an error estimate of 25%.

4. Theoretical calculation

The cross sections for electron-impact excitation of atomic oxygen were calculated in the *R*-matrix with pseudostates (RMPS) approach using the *R*-matrix package RMATRIX1 (Berrington *et al* 1995). We included 18 bound states, 4 autoionizing states and 19 pseudostates in the close-coupling expansion. The autoionizing states exhibit strong dipole coupling with the ground and some other low lying bound states. The importance of coupling to the continuum states for electron-impact excitation of atomic oxygen has been discussed by Tayal (2002). The cross sections for the $2s^2 2p^4\ ^3P \rightarrow 2p^3 3s\ ^3S^o$ transition were reduced by 5–15% due to the coupling of bound states to the continuum target states. The pseudostates are included to simulate the effect of continuum target states and, thus, to allow for loss of flux into the infinitely dipole-coupled states. The computational details of the collision calculation have been given by Tayal (2002). Here we present a brief outline. Accurate description of target wavefunctions is an essential component of any reliable scattering calculation. All target states have been represented by configuration-interaction (CI) wavefunctions. Our wavefunctions adequately account for the main correlation corrections and the strong interactions between different $2s^2 2p^3 nl$ Rydberg series and the $2s2p^5$ perturbers.

Fifteen orthogonal one-electron orbitals, 1s, 2s, 2p, 3s, 3p, 3d, 4s, 4p, 4d, 4f, 5s, $\overline{5p}$, $\overline{5d}$, $\overline{6s}$ and $\overline{7s}$, have been used to construct the CI functions of the target states. The 1s, 2s and 2p radial functions were taken from the table given by Clementi and Roetti (1974). The radial functions 3s, 3p, 3d, 4s, 4p, 4d, 4f and 5s are chosen as spectroscopic type and were optimized on the $2p^3 3s$, $2p^3 3p$, $2p^3 3d$, $2p^3 4s$, $2p^3 4p$, $2p^3 4d$, $2p^3 4f$ and $2p^3 5s$ excited states, using the structure package CIV3 (Hibbert 1975). The pseudo-orbitals $\overline{5p}$, $\overline{5d}$, $\overline{6s}$ and $\overline{7s}$ were optimized on the $2p^3 3p\ ^3P$, $2p^3 3d\ ^3D^o$, $2p^3 3s\ ^3S^o$ and $2p^3 3s\ ^5S^o$ states, respectively, to approximately represent higher bound plus continuum parts of the series. The autoionizing states $2p^3 3s\ ^3P^o$, $2s2p^5\ ^3P^o$, $2p^3 3d\ ^3P^o$ and $2p^3 4d\ ^3P^o$ simulate a part of the coupling to the continuum. The 41 target states included in our scattering calculation are listed in table 1 where calculated excitation energies are compared with the best available experimental values from the National Institute of Standards and Technology (NIST) compilation (Weise *et al* 1996; NIST Atomic Spectra Database, http://physics.nist.gov). There is very good agreement between the calculated and measured values, indicating a good quality of target wavefunctions used in the scattering calculation. An *R*-matrix radius of 61.6 atomic units (au) was required to accommodate all the fifteen physical and pseudo-orbitals. Seventy-two continuum basis functions were used for each angular momentum. The calculated target state energies for the physical states were adjusted to the measured values prior to the diagonalization of the Hamiltonian matrices.

5. Results

The experimentally and theoretically determined DCSs at energies between 15 and 27.5 eV are presented in figure 2. Also shown are the available data from other groups. For convenience,

Table 1. Target states included in the RMPS calculation with excitation energies relative to the ground state.

State index	*LS* state	Energy (eV) Present	Observed	State index	*LS* state	Energy (eV) Present
1	$2s^22p^4\ ^3P$	0	0	23	$2s^22p^3(^4S^o)\overline{6s}\ ^5S^o$	17.58
2	$2s^22p^3(^4S^o)3s\ ^5S^o$	9.23	9.14	24	$2s^22p^3(^4S^o)\overline{6s}\ ^3S^o$	18.59
3	$2s^22p^3(^4S^o)3s\ ^3S^o$	9.67	9.51	25	$2s^22p^3(^2D^o)\overline{5d}\ ^3D^o$	21.14
4	$2s^22p^3(^4S^o)3p\ ^5P$	10.91	10.73	26	$2s^22p^3(^2P^o)\overline{6s}\ ^3P^o$	23.38
5	$2s^22p^3(^4S^o)3p\ ^3P$	11.24	10.98	27	$2s^22p^3(^4S^o)\overline{5d}\ ^5D^o$	29.10
6	$2s^22p^3(^4S^o)4s\ ^5S^o$	11.96	11.83	28	$2s^22p^3(^2D^o)\overline{6s}\ ^3D^o$	29.88
7	$2s^22p^3(^4S^o)4s\ ^3S^o$	12.07	11.92	29	$2s^22p^3(^2D^o)\overline{5d}\ ^3D^o$	32.66
8	$2s^22p^3(^4S^o)3d\ ^5D^o$	12.22	12.07	30	$2s^22p^3(^2D^o)\overline{5d}\ ^3S^o$	33.00
9	$2s^22p^3(^4S^o)3d\ ^3D^o$	12.23	12.08	31	$2s^22p^3(^2D^o)\overline{5d}\ ^3P^o$	33.09
10	$2s^22p^3(^4S^o)4p\ ^5P$	12.43	12.28	32	$2s^22p^3(^2P^o)\overline{5d}\ ^3P^o$	34.81
11	$2s^22p^3(^4S^o)4p\ ^3P$	12.59	12.35	33	$2s^22p^3(^2P^o)\overline{5d}\ ^3D^o$	34.93
12	$2s^22p^3(^2D^o)3s\ ^3D^o$	12.82	12.53	34	$2s^22p^3(^4S^o)\overline{5p}\ ^5P$	36.06
13	$2s^22p^3(^4S^o)5s\ ^5S^o$	12.88	12.65	35	$2s^22p^3(^4S^o)\overline{5p}\ ^3P$	37.95
14	$2s^22p^3(^4S^o)5s\ ^3S^o$	12.89	12.69	36	$2s^22p^3(^4S^o)\overline{7s}\ ^5S^o$	41.47
15	$2s^22p^3(^4S^o)4d\ ^5D^o$	12.92	12.72	37	$2s^22p^3(^2P^o)\overline{5p}\ ^3P$	43.46
16	$2s^22p^3(^4S^o)4d\ ^3D^o$	13.01	12.75	38	$2s^22p^3(^4S^o)\overline{7s}\ ^3S^o$	45.02
17	$2s^22p^3(^4S^o)4f\ ^5F$	13.04	12.76	39	$2s^22p^3(^2D^o)\overline{7s}\ ^3D^o$	45.59
18	$2s^22p^3(^4S^o)4f\ ^3F$	13.16	12.76	40	$2s^22p^3(^2P^o)\overline{7s}\ ^3P^o$	47.78
19	$2s^22p^3(^2P^o)3s\ ^3P^o$	14.01	14.12	41	$2s^22p^3(^2D^o)\overline{5p}\ ^3P$	51.13
20	$2s^2p^5\ ^3P^o$	15.65	15.65	—	—	—
21	$2s^22p^3(^2D^o)3d\ ^3P^o$	16.69	—	—	—	—
22	$2s^22p^3(^2D^o)4d\ ^3P^o$	17.08	—	—	—	—

the measured data are tabulated in table 2. The table also includes recommended absolute DCSs beyond the measured angular range. Following Kanik *et al* (2001), these values are chosen on the basis of the general trends of the measured data along with the angular behaviour of the RMPS data. They are used to generate the ICSs as discussed earlier. Error estimates are only listed for the measured data. The ICS data are plotted in figure 3 along with data from earlier work. Both the experimental and theoretical ICS data are included in table 2.

6. Discussion

It is clear from figure 2 that there is good agreement in shape between our experimental and RMPS DCS data in the angular region of overlap, though the experimental results tend to lie slightly lower in absolute magnitude. However, the experimental and theoretical DCS data are in agreement within the quoted errors in most instances. The trend for the theoretical data to be larger was also observed in our earlier work at higher energies (Kanik *et al* 2001) but to a greater degree. This improvement in absolute agreement between the RMPS data and the *R*-matrix data of Kanik *et al* (2001) can be attributed to the refinements of the RMPS method over the *R*-matrix calculation of Kanik *et al* (2001).

The only other experimental DCS data in this energy region are presented in a series of papers from Doering and co-workers (Vaughan and Doering (1987) (16.5, 20 and 25 eV), Gulcicek and Doering (1988) (13.87, 16.5, 20 eV) and Doering and Yang (2001) (13.4, 18.6 and 23.6 eV)). These data are also plotted in figure 2. Unfortunately, there is not an exact

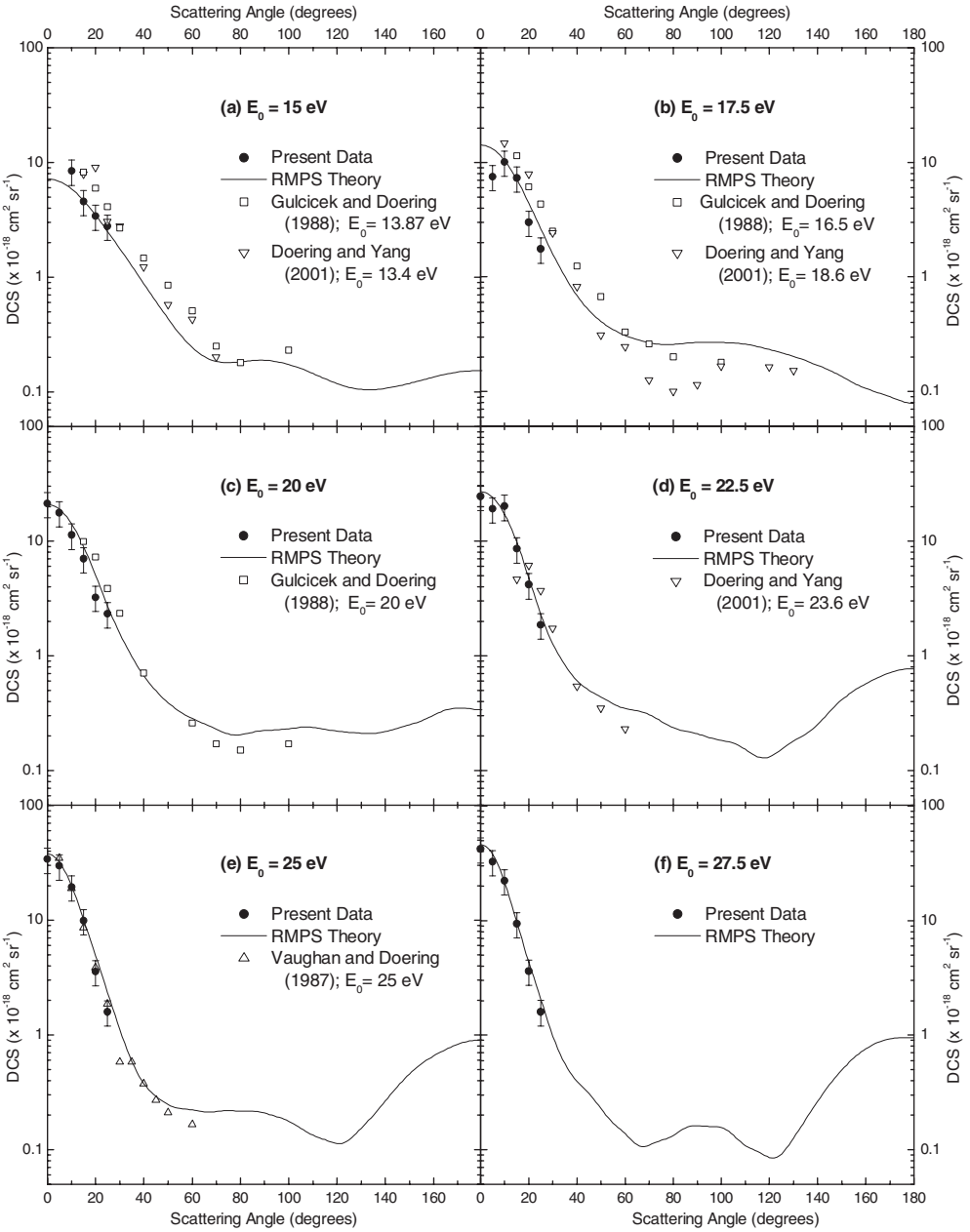

Figure 2. Experimental and theoretical DCSs for $2s^2 2p^4\ ^3P \rightarrow 2p^3 3s\ ^3S^o$ excitation at the energies indicated. The results of Vaughan and Doering (1987) (25 eV), Gulcicek and Doering (1988) (13.87, 16.5, 20 eV) and Doering and Yang (2001) (13.4, 18.6 and 23.6 eV) are also shown. Where an exact correlation in impact energy between data sets does not exist, we have plotted the data sets which most closely match for a rough comparison. All impact energies are clearly indicated in the figure.

correlation between the energies investigated in the present study and those investigated by Doering and co-workers. However, where an exact correlation between data sets does not exist,

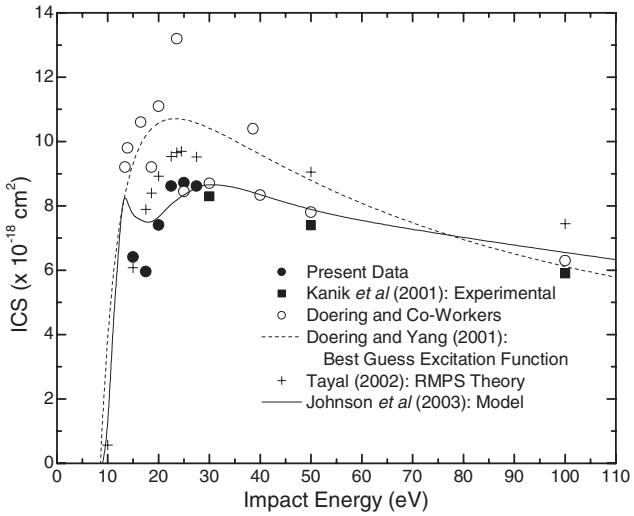

Figure 3. Experimental and theoretical ICSs for the $2s^2 2p^4\ ^3P \rightarrow 2p^3 3s\ ^3S^o$ excitation are plotted alongside those of Kanik *et al* (2001) and Doering and co-workers (Vaughan and Doering (1986) (40 eV), Vaughan and Doering (1987) (25, 30, 50, 100 eV), Gulcicek and Doering (1988) (13.87, 16.5, 20 eV) and Doering and Yang (2001) (13.4, 18.6, 23.6 eV and the 'best guess' excitation function)). The model results of Johnson *et al* (2003) are also plotted. Error bars have not been included to reduce congestion of the figure.

we have plotted the data sets which most closely match for a rough comparison. The impact energies of the all data sets are clearly indicated on the figure. Furthermore, in plotting the data of Doering and co-workers, we have assumed that where two data sets occur at the same energy, the more recent supersedes the other. Thus, at 20 eV, we plot the Gulcicek and Doering (1988) data rather than the Vaughan and Doering (1987) data.

A number of points can be made regarding a comparison of the different data sets. First, our data lie consistently lower than the Doering data at virtually all angles and energies, though the shapes of the DCS are very similar. The same trend has previously been observed at higher energies (30, 50 and 100 eV; Kanik *et al* 2001), while the largest discrepancies occur at the lowest energies (15 and 17.5 eV). Nonetheless, the differences between the two data sets are smaller than the combined error bars at all energies. Second, there is quite good agreement in shape between the Doering results and our RMPS data. The higher angle oscillations in the RMPS DCS data reproduce those seen in the Doering results quite well, adding further validity to our procedure for determining the relative values of the DCSs at high angles.

The ICSs are displayed in figure 3. In addition to the current low energy data, we present the higher energy data (30, 50 and 100 eV) of Kanik *et al* (2001) for completeness. The current ICSs, combined with those of Kanik *et al* (2001), show a smooth excitation function over the full range of impact energies represented. The results of Doering and co-workers, along with the RMPS ICS data of Tayal (2002), are also shown in figure 3. The *R*-matrix results of Kanik *et al* (2001) are not included as the RMPS results of Tayal (2002) supersede them. The solid curve shown in figure 3 is taken from Johnson *et al* (2003) and is the result of a model calculation in which the excitations of 60 atomic oxygen states are considered simultaneously. For further details of the model and how the cascade is considered, the reader is referred to Johnson *et al* (2003) and Shemansky and Liu (2003).

The following points should be noted from figure 3. The cross section is observed to rise steeply from threshold to a maximum near 25 eV. This maximum is observed in both

Table 2. Electron-impact DCSs and ICSs for the $2s^2 2p^4\ ^3P \rightarrow 2p^3 3s\ ^3S^o$ excitation in atomic oxygen.

Scattering angle (deg)	DCS (10^{-18} cm^2 sr^{-1})					
	$E_0 = 15$ eV	$E_0 = 17.5$ eV	$E_0 = 20$ eV	$E_0 = 22.5$ eV	$E_0 = 25$ eV	$E_0 = 27.5$ eV
0	7.62	10.72	21.3 ± 5.33	24.6 ± 6.14	34.0 ± 8.50	42.1 ± 10.53
5	7.23	7.50 ± 1.87	17.7 ± 4.42	19.1 ± 4.78	29.8 ± 7.45	32.5 ± 8.13
10	8.43 ± 2.11	10.1 ± 2.53	11.3 ± 2.83	20.1 ± 5.03	19.5 ± 4.87	22.3 ± 5.57
15	4.58 ± 1.15	7.30 ± 1.83	7.01 ± 1.75	8.59 ± 2.15	9.92 ± 2.48	9.41 ± 2.35
20	3.41 ± 0.85	3.01 ± 0.75	3.23 ± 0.81	4.18 ± 1.01	3.56 ± 0.89	3.63 ± 0.91
25	2.79 ± 0.70	1.75 ± 0.44	2.33 ± 0.58	1.86 ± 0.47	1.59 ± 0.40	1.60 ± 0.40
30	1.87	1.20	1.30	1.15	1.51	0.89
40	0.93	0.52	0.56	0.55	0.51	0.36
50	0.46	0.31	0.33	0.40	0.34	0.21
60	0.26	0.23	0.24	0.31	0.30	0.12
70	0.19	0.20	0.19	0.28	0.29	0.10
80	0.19	0.19	0.17	0.21	0.29	0.12
90	0.20	0.20	0.19	0.19	0.28	0.15
100	0.18	0.20	0.19	0.17	0.24	0.14
110	0.15	0.20	0.20	0.14	0.18	0.10
120	0.12	0.18	0.18	0.12	0.15	0.08
130	0.11	0.15	0.18	0.16	0.21	0.11
140	0.11	0.13	0.18	0.23	0.36	0.24
150	0.13	0.10	0.21	0.37	0.62	0.45
160	0.14	0.08	0.25	0.52	0.89	0.69
170	0.16	0.07	0.29	0.65	1.13	0.84
180	0.16	0.06	0.28	0.70	1.23	0.86
ICS(experiment)[a]	6.41 ± 1.60	5.96 ± 1.49	7.41 ± 1.85	8.62 ± 2.15	8.72 ± 2.18	8.62 ± 2.15
ICS(theory)[a]	6.08	7.89	8.93	9.54	9.70[b]	9.53

[a] ICSs in units of 10^{-18} cm^2.
[b] Calculated at 24.5 eV impact energy.

the RMPS and the present experimental data, while the model calculations of Johnson *et al* (2003) indicate a maximum near 30 eV. An initial local maximum is seen at lower energies of the model calculation results (Johnson *et al* 2003). A hint of this maximum is also seen in the present ICS data. The reason for such a maximum is not clear. The data from the various Doering experiments are very scattered in the low energy region though the 'best guess' excitation function of Doering and Yang (2001) indicates a maximum in the excitation function near 20 eV. For other arguments relating to the cross section proposed by Doering and Yang (2001) and a summary of the normalization procedures employed by Doering and co-workers, see Kanik *et al* (2001). Regarding the absolute magnitude of the cross section at its maximum, our data support a value of $(8.7 \pm 2.2) \times 10^{-18}$ cm^2.

7. Conclusions

We have presented absolute ICSs and DCSs for the $2s^2 2p^4\ ^3P \rightarrow 2p^3 3s\ ^3S^o$ transition in atomic oxygen at energies of 15, 17.5, 20, 22.5, 25 and 27.5 eV. Experimental DCS data were obtained at angles between 0° and 25° while RMPS calculations are presented for the complete angular range. The shapes of the DCSs were very consistent in the angular range of overlap and agreed within quoted uncertainties at virtually all comparable energies and angles. Good agreement

in the shapes of the DCSs was also obtained with the data of Doering's group. ICSs, derived from the relative DCSs, are presented and support a slower rise of the cross section above threshold than had been suggested recently by Doering and Yang (2001).

Acknowledgments

The measurements were carried out at the Jet Propulsion Laboratory, California Institute of Technology, and were supported by the NASA Astrophysics and Planetary Atmospheres Program Offices. PVJ gratefully acknowledges financial support from the Research Associateship Program of the National Research Council. MAK acknowledges support from a NASA Summer Faculty Fellowship (2002) and NSF for this work. JWMcC acknowledges support from NSERC (Canada). The research at Clark Atlanta University (SST) was supported by NASA Grant NAG5-13340 from the Planetary Atmospheres Program.

References

Berrington K A, Eissner W B and Norrington P H 1995 *Comput. Phys. Commun.* **92** 290
Clementi E and Roetti C 1974 *At. Data Nucl. Data Tables* **14** 177
Doering J P and Yang J 2001 *J. Geophys. Res.* **106** 203
Gulcicek E E and Doering J P 1988 *J. Geophys. Res.* **93** 5879
Hibbert A 1975 *Comput. Phys. Commun.* **9** 141
Hughes M, James K E Jr, Childers J G and Khakoo M A 2003 *Meas. Sci. Technol.* **14** 841
Johnson P V and Kanik I 2001 *J. Phys. B: At. Mol. Opt. Phys.* **34** 3041
Johnson P V, Kanik I, Shemansky D E and Liu X 2003 *J. Phys. B: At. Mol. Opt. Phys.* **36** 3203
Kanik I, Johnson P V, Das M B, Khakoo M A and Tayal S S 2001 *J. Phys. B: At. Mol. Opt. Phys.* **34** 2647
Noren C, Kanik I, Johnson P V, McCartney P, James G K and Ajello J M 2001 *J. Phys. B: At. Mol. Opt. Phys.* **34** 2667
Shemansky D E and Liu X 2003 *J. Geophys. Res.* to be submitted
Shyn T W, Sweeney C J and Grafe A 1994 *Phys. Rev.* A **49** 3680
Tayal S S 2002 *Phys. Rev.* A **66** 030701(R)
Trajmar S and Kanik I 1995 *Atomic and Molecular Processes in Fusion Edge Plasmas* ed R K Janev (New York: Plenum) pp 31–58
Trajmar S and Register D F 1984 *Electron Molecule Collisions* ed K Takayanagi and I Shimamura (New York: Plenum) pp 427–93
Vaughan S O and Doering J P 1986 *J. Geophys. Res.* **91** 13755
Vaughan S O and Doering J P 1987 *J. Geophys. Res.* **92** 7749
Weise W L, Fuhr J R and Deters T M 1996 *J. Phys. Chem. Ref. Data Monogr.* **7** 335